Nonlinear Waves in Subwavelength Waveguide Arrays: Evanescent Bands and the "Phoenix Soliton"

Or Peleg,[1] Mordechai Segev,[1] Guy Bartal,[2] Demetrios N. Christodoulides,[3] and Nimrod Moiseyev[1,4]

[1]*Physics Department, Technion - Israel Institute of Technology, Haifa 32000, Israel*

[2]*NSF Nanoscale Science and Engineering Center (NSEC), University of California, Berkeley, California 94720-1740, USA*

[3]*College of Optics & Photonics—CREOL, University of Central Florida, Orlando, Florida 32816, USA*

[4]*Chemistry Department, Technion - Israel Institute of Technology, Haifa 32000, Israel*

(Received 21 August 2008; published 23 April 2009)

We formulate wave propagation in arrays of subwavelength waveguides with sharp index contrasts and demonstrate the collapse of bands into evanescent modes and lattice solitons with superluminal phase velocity. We find a self-reviving soliton ("phoenix soliton") comprised of coupled forward- and backward-propagating light, originating solely from evanescent bands. In the linear regime, all Bloch waves comprising this beam decay, whereas a proper nonlinearity assembles them into a propagating self-trapped beam. Finally, we simulate the dynamics of such a beam and observe breakup into temporal pulses, indicating a new kind of slow-light gap solitons, trapped in time and in one transverse dimension.

DOI: 10.1103/PhysRevLett.102.163902 PACS numbers: 42.65.Tg, 42.50.Md, 42.65.Hw, 42.70.Qs

The propagation of electromagnetic (EM) waves in waveguide arrays has been studied extensively, under the assumption that the width of each waveguide is larger than the optical wavelength [1]. When, in addition, the refractive index contrast is small, light propagation in waveguide arrays is equivalent to dynamics of quantum-mechanical wave packets in a periodic potential. This insight led to analogies between optics and solid-state physics [2,3], e.g., photonic crystals [4], optical Bloch waves [5], Bloch oscillations [6], Brillouin-zone spectroscopy [7], and Zener tunneling [8]. These ideas, with many more in the nonlinear domain, rely on equivalence between the paraxial wave equation and the Schrödinger equation [3]. However, recent technology advances enable fabricating waveguides narrower than the optical wavelength, and with a very large index contrast (~2–3) [9]. In such structures, the wave varies at the scale of the array; hence, neither the paraxial approximation nor the scalar Helmholtz equation is valid. Previous studies on optical nanostructures addressed form birefringence [10], low-index guiding [9], optical forces on waveguides [11], and nonlinear effects such as two-photon absorption [12], Raman amplification [13], and supercontinuum generation [14]. However, merging the two areas—nonlinear dielectric waveguide arrays and subwavelength structures—has not been addressed.

Here we formulate wave propagation in waveguide arrays with subwavelength periodicity and a very large refractive index contrast. We use non-Hermitian operator theory, find the Bloch modes, and demonstrate collapse of propagating modes into evanescent waves, forming bands of imaginary propagation constants separated by gaps. We find Bloch modes and solitons with superluminal phase velocities: extended and self-localized states propagating with an effective index between zero and one. We demonstrate "phoenix solitons": solitons originating solely from evanescent waves; in the linear regime, this beam decays exponentially, whereas at a proper nonlinearity, the beam becomes a propagating soliton, comprised of coupled forward and backward modes. In simulating the dynamics of such self-localized beams, we observe a breakup into temporal pulses arising from spatiotemporal modulation instability, providing evidence of a new kind of gap solitons, trapped both in time and in a transverse dimension and propagating at extremely slow group velocities. These solitons are fundamentally different from all gap solitons investigated thus far [15], and they provide a vision for the existence of bullet lattice solitons.

When the refractive index and the optical field vary rapidly at a subwavelength scale, scalar field approximations are invalid (where longitudinal components of the fields are neglected). One should solve Maxwell's equations jointly for the electric and magnetic fields [16]. Here we solve for a 1D waveguide array with a refractive index periodic in x and uniform in the propagation direction z. The standard procedure for such 1D problems is to solve for the longitudinal electric (magnetic) field in the TM (TE) polarization in each section separately and tailor the boundary conditions [17] or to use the matching condition to discretize the equations [5]. However, we would like to obtain a propagation equation that incorporates the boundary conditions and to obtain an initial-value problem. Our formalism produces two coupled first-order differential equations. (In order to solve for the TM polarizations, we used the continuity of the transverse displacement electric field to determine the expression of the derivatives in the boundary points of the numerical grid.) We emphasize that, due to the small features of the array (the periodicity can take any value) and the high-index contrast, the second derivatives in z cannot be neglected. For a monochromatic wave, and for TM polarization, we find, following Ref. [16],

$$i\frac{\partial}{\partial z}\begin{pmatrix} E \\ H \end{pmatrix} = k_0 \begin{pmatrix} 0 & 1+\frac{1}{k_0^2}\frac{\partial}{\partial x}\left(\frac{1}{\varepsilon}\frac{\partial}{\partial x}\right) \\ \varepsilon & 0 \end{pmatrix}\begin{pmatrix} E \\ H \end{pmatrix} = \begin{pmatrix} 0 & A \\ B & 0 \end{pmatrix}\begin{pmatrix} E \\ H \end{pmatrix} \equiv M\Psi. \quad (1)$$

E and H are the spatial parts of the time-harmonic electric and magnetic fields, in the x and y directions, respectively, Ψ is the (E, H) vector, k_0 is the vacuum wave number, and ε is the relative dielectric coefficient, with $\varepsilon(x) = \varepsilon_0 + \Delta\varepsilon_L(x)$, where $\Delta\varepsilon_L(x) = \Delta\varepsilon_L(x + D)$, D being the lattice periodicity. We emphasize that the matrix operator M acting on Ψ is non-Hermitian. Describing wave propagation through M brings naturally evanescent waves, because the eigenvalues of M can be complex. This is in contrast to the modal solutions of the Helmholtz equation, which become evanescent through an external condition $k_z{}^2 < 0$ [k_z being the wave number in the propagation direction z], not as a natural outcome of the propagation equation.

Since $n(x)$ is periodic, the operator M has discrete translation invariance; hence, its linear eigenmodes are Bloch waves, whose eigenvalues (propagation constants), albeit being complex, are arranged in bands separated by gaps. Seeking eigenmodes, we set $\tilde{\Psi} = \Psi_{mk}(x)e^{i(\beta z + kx)}$, where k is the Bloch wave number, m is the band number, and $\Psi_{mk}(x) = \Psi_{mk}(x + D)$. We solve the resulting eigenvalue equation for β and find that the values are either real (propagation modes) or imaginary (evanescent modes) but never complex (no leaky modes, as the array is infinite in x). Since the second derivative in z is not neglected, the modes appear in pairs: forward-evolving and backward-evolving modes. The forward-evolving propagation modes have $\beta > 0$, whereas the backward-evolving propagation modes have $\beta < 0$. Likewise, the evanescent modes have $\beta = -i\tilde{\beta}$, where $\tilde{\beta}$ is real, and $\tilde{\beta} > 0$ ($\tilde{\beta} < 0$) for the forward- (backward-) evolving modes.

Consider first the forward-evolving modes. Their propagation constants are arranged in a finite number of propagation bands of real β, while at some cutoff value of k (denoted as k_{co}) one of the higher bands "collapses," yielding $\beta = 0$ at k_{co} (actually, k_{co} is a mathematical branch point; see the upper row of Fig. 1). Interestingly, at the branch point k_{co} the corresponding Bloch mode is orthogonal to itself, as a consequence of the coalescence of two orthogonal states [18]. From k_{co} and on, the values of β are imaginary: Bloch modes with $k > k_{\mathrm{co}}$ are evanescent [e.g., band 3 in Fig. 1(b)]. The evanescent modes, albeit having imaginary β's, are still organized in bands separated by gaps [Fig. 1]. As the periodicity D is decreased, the collapse occurs at lower bands, until band 1 alone has propagating waves, and all of the other bands are evanescent. If we further decrease D, k_{co} occurs within band 1, which can be divided into three regimes: subluminal propagation modes with $\beta > k_0$, superluminal propagation (not evanescent) modes with $\beta < k_0$ and hence superluminal phase velocity ($0 < n_{\mathrm{eff}} < 1$), and evanescent modes with imaginary β's. The boundaries of each region can be deduced analytically [5].

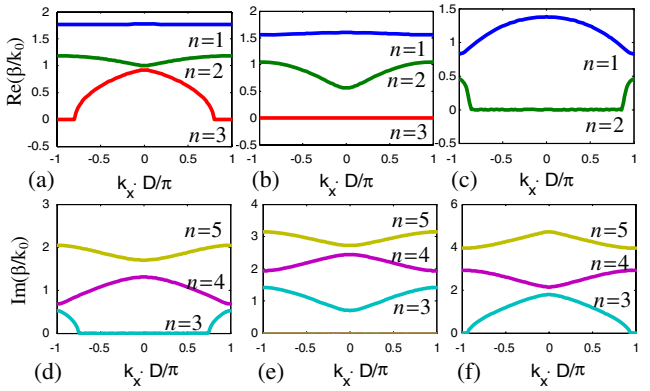

FIG. 1 (color online). Band structure of the 1D waveguide array, with the band number indicated at each curve. (a)–(c) Real and (d)–(f) imaginary parts of the propagation constant for refractive indices 2 and 1, $\lambda = 1.5$ μm, and periodicity (a), (d) 1400, (b),(e) 1000, and (c),(f) 600 nm.

When D is very small, the amplitudes of the TM modes at the edge of band 1 have their zero crossings in the high-index region (as opposed to low-contrast waveguides, where zero crossings are between waveguides). This has strong implications especially for the nonlinear case, since the region of higher intensity will be in the lower index region for TM, whereas for TE it resides in the higher index region. Hence, TE and TM modes behave entirely differently under nonlinearity, which can be utilized to construct efficient nonlinear polarization switches.

Since M is not Hermitian, its eigenvectors are not orthogonal according to the ordinary inner product. Instead, they obey biorthogonality, for which we define left and right states [19]:

$$M\psi^R_{mk} = \beta_{mk}\psi^R_{mk}, \qquad M^T\psi^L_{mk} = \beta_{mk}\psi^L_{mk},$$

where $\Psi^R{}_{mk}$ ($\Psi^L{}_{mk}$) is the eigenvector of M (M^T, the transposed of M). The orthogonality relation is $\langle\Psi^L{}_{m'k'}|\Psi^R{}_{mk}\rangle = \int\Psi^L{}_{m'k'}\Psi^R{}_{mk}dx = \delta_{mm'}\delta_{(k-k')}$. The left states are the back-propagating modes (evolving in the $-z$ direction). Notice the branch point at k_{co}, where the eigenvalues coincide and the eigenvectors are self-orthogonal [18]. Here M is traceless; hence, this branch point appears when $\beta = 0$ [20], corresponding to coalescence of the forward- and backward-propagating waves. The branch point renders the Bloch basis incomplete; however, numerical inaccuracies enable using it as a complete basis [18]. Thus, using biorthogonality, we can *uniquely decompose any EM field* propagating in the array into propagating and evanescent Bloch modes.

We proceed to nonlinear effects. The third-order polarization yields $\vec{P}_{\mathrm{NL}} = (1/2)\varepsilon_0\chi^{(3)}[|\vec{E}|^2\vec{E} + (1/2)\cdot(\vec{E}\cdot\vec{E})\vec{E}^*]$, the last term describing coupling between longitudinal and transverse components of $\vec{E}$. This expression is valid even for a large nonlinearity, as long as its source is

bound electrons [21]. With the nonlinear addition, the operator M retains its shape, but A and B are redefined. We find solitons by solving the nonlinear equation self-consistently [22].

To illustrate the strong nonlinear birefringence of the system, we note that, when only the low-index material is nonlinear, TE and TM solitons have substantially different widths: e.g., 20 μm for the TM soliton against 70 μm for the TE soliton, for a soliton from the edge of band 1. This happens because the peak intensity of the TM mode is in the low-index material, whereas the peak intensity of the TE mode is in the high-index medium. After finding a soliton, we simulate its propagation by dividing the dynamics into two parts [16]: linear propagation, by projecting the field onto the Bloch modes (each accumulating phase according to its β), and nonlinear propagation, calculated through an operator M_{NL} containing just the nonlinear contributions to M. This procedure works well as long as the forward-propagating field has no contribution from the backward-propagating modes. Here this procedure can be used to find solitons as long as the Bloch modes comprising them are not evanescent (the latter cases are addressed later on).

As an example, we set D to have a single propagation band, and the branch point appears in the gap between bands 1 and 2. A soliton arising from the edge of band 1 is supported by a negative nonlinearity (since it arises from the anomalous diffraction region), and its propagation constant is smaller than k_0. That is, the soliton has a superluminal phase velocity. Figure 2 shows the simulated propagation of this beam. The nonlinearity is strong (index change $\sim$0.01), yet the soliton width is rather large ($\sim 8\lambda$), because the nonlinearity has to balance a huge diffraction. The diffraction length of such a wave packet is merely 50 μm, which is the consequence of the strong coupling between the waveguide channels near the edge of band 1. The propagation constant of this soliton is $0.65k_0$, as determined by D and the nonlinearity: a smaller D yields a smaller propagation constant. One can tune parameters to have a very small propagation constant, but in practice the limitation is fabrication accuracy, limiting the ability to tune the edge of band 1. In addition, the smaller the region of anomalous diffraction within band 1, the stronger the diffraction near the band edge. Thus, the width of the soliton at a given nonlinearity increases as we decrease the anomalous diffraction region within band 1. Such superluminal phase velocity (which could be extremely large) is a very large wavelength inside the array.

Setting the cutoff to the edge of band 2 ($k_{\mathrm{co}} = \pi/D$) has intriguing implications on a beam arising exactly from that point. Linearly, under these conditions, any combination of eigenmodes from band 2 decays exponentially, because they all have imaginary propagation constants. But when nonlinearity is introduced, the modes can form a superposition propagating in unison, having a single, real, propagation constant. That is, the wave packet becomes a propagating eigenmode of the nonlinear operator—a phoenix soliton—which is propagating without any decay or diffraction broadening. This soliton is completely different from any other soliton. In the absence of nonlinearity, this beam experiences exponential decay. But when nonlinearity is introduced, the phoenix soliton, arising from the evanescent modes, "carves" its way and traverses the array without a change in shape. This dramatic change of behavior stems from setting band 2 to just turn fully evanescent. Projecting this soliton on the linear modes of the system yields significant projections on both forward and backward evanescent modes [Fig. 3(b)]. The envelope of a phoenix soliton is rather large [$\sim 6.5\lambda$, Fig. 3(a)]; however, it has a fine subwavelength structure. To launch this phoenix soliton, one should excite *solely* evanescent modes, without *any* propagating mode. For the example of Fig. 3, the propagation constant is $0.083k_0$, under a strong nonlinearity ($\Delta n \sim 5 \times 10^{-2}$, the intensity is always normalized to 1, whereas the strength of the nonlinearity enters only through Δn). However, one could use a much weaker nonlinearity, yielding a broader soliton with similar subwavelength features.

A phoenix soliton has significant projections on both forward and backward evanescent modes [Fig. 3(b)], as opposed to all previously studied gap solitons, which were made up of propagating modes [15]. Hence, one cannot simulate its propagation with any method relying on solving an initial-value problem. Instead, we use the RSOFT© finite difference time domain (FDTD) software, which solves Maxwell's equations in time and space. Such a simulation also includes the temporal dynamics of the EM wave. The spatial propagation dynamics of the

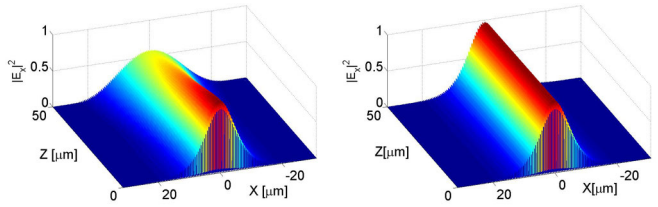

FIG. 2 (color online). Superluminal propagation arising from the bottom of band 1 ($D = 500$ nm). (a) Linear diffraction. (b) Soliton propagation.

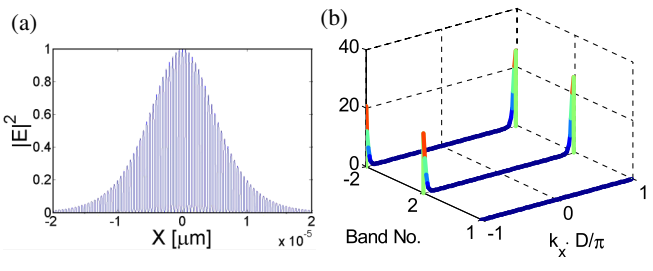

FIG. 3 (color online). (a) Intensity structure of the phoenix soliton (TE polarization), and (b) its projections on the bands: the first and second forward-propagating and backward-propagating bands.

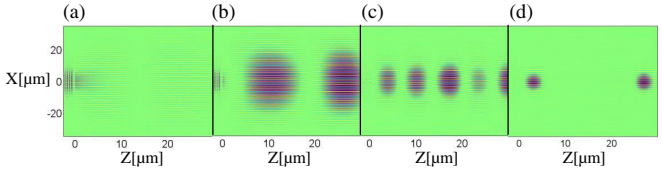

FIG. 4 (color online). Propagation of the phoenix soliton under various nonlinearity strengths. The real part of the electric field is shown as a function of x and z at a specific time t_0. (a) Linear propagation. (b) $n_2 = 0.1$. (c) $n_2 = 0.3$. (d) $n_2 = 0.5$.

phoenix soliton, at some specific time t_0, is depicted in Fig. 4. For simplicity, we have chosen a TE polarization for the soliton, and only the high refractive index medium is nonlinear. The parameters of the input beam are those of the soliton of Fig. 3, launched into the array through a bulk medium with a refractive index of 2. To make the simulation more stable, we use a saturable nonlinearity of the form $\chi^{(3)}|E|^2/(1 + I_{\mathrm{sat}})$, and I_{sat} is the saturation intensity. Linearly, the beam is totally reflected from the input plane of the array, and no intensity reaches the end face [Fig. 4(a)]. As we gradually increase the nonlinearity [Fig. 4(b)], the beam self-focuses in the transverse dimension, and it starts propagating through the array with less loss, because most of its modal constituents have transformed from evanescent to propagating modes. In addition, the EM field forms temporal pulses. As we further increase the nonlinearity, we notice that the beam self-focuses to narrower width, and at the same time the temporal pulses it forms are narrower. Notice also that the distance between consecutive field maxima gets larger with increasing nonlinearity. As the nonlinearity reaches the appropriate value to form the phoenix soliton of Fig. 3, the beam self-traps in space, traversing the array with only minor changes in its shape [Fig. 4(c)]. The temporal pulses emerging from this FDTD simulation are the outcome of spatiotemporal modulation instability, which is a precursor to spatiotemporal solitons. Evidently, the launched beam is evolving into solitons that are trapped not only in the transverse dimension x but also in time: $(1 + 1 + 1)$-dimensional spatiotemporal gap solitons [Fig. 4(d)]. These self-forming temporal pulses are moving extremely slowly, reaching a velocity of $0.025c$. The self-trapping in time arises from the balance between nonlinearity and the huge grating dispersion of the array with subwavelength periodicity. All of these features make the phoenix soliton fundamentally different from any other spatiotemporal gap (or Bragg) soliton [15].

In conclusion, we formulated the theory of wave propagation in a subwavelength waveguide array and predicted new entities with no counterpart in homogeneous systems or in larger-than-wavelength arrays. We proposed solitons arising solely from evanescent waves and observed numerically that they form narrow temporal pulses, propagating at very slow group velocities. These self-formed pulses, together with the self-channeling in the transverse dimension, are a direct indication of the existence of gap solitons trapped both in time and in the transverse dimension. The subwavelength features of such $(1 + 1 + 1)$-dimensional gap solitons are fundamentally different from their bulk counterparts [23], even though both entities are self-trapped both in time and in one transverse dimension. With the recent advances in technology [24], such a subwavelength array can be fabricated also in 2D, which would provide a method to generate "gap light bullets," trapped in time and in both transverse dimensions, similar to their long-sought bulk counterparts [25]. Additionally, our study paves the way to many intriguing ideas that should exhibit unique features on the subwavelength scales: from instabilities and shock waves to self-pulsation and self-organization.

This work was supported by the U.S.–Israel Binational Foundation, Israel Science Foundation, and an ERC advanced grant.

[1] A. Yariv, *Optical Elecronics in Modern Communications* (Oxford University Press, New York, 1997).
[2] P. St. J. Russell, Appl. Phys. B **39**, 231 (1986).
[3] D. N. Christodoulides *et al.*, Nature (London) **424**, 817 (2003).
[4] E. Yablonovitch, Phys. Rev. Lett. **58**, 2059 (1987).
[5] P. Yeh and A. Yariv, J. Opt. Soc. Am. **67**, 423 (1977).
[6] T. Pertsch *et al.*, Phys. Rev. Lett. **83**, 4752 (1999); R. Morandotti, Phys. Rev. Lett. **83**, 4756 (1999).
[7] G. Bartal *et al.*, Phys. Rev. Lett. **94**, 163902 (2005).
[8] H. Trompeter *et al.*, Phys. Rev. Lett. **96**, 053903 (2006).
[9] Q. Xu *et al.*, Opt. Lett. **29**, 1626 (2004).
[10] I. Richter *et al.*, Appl. Opt. **34**, 2421 (1995).
[11] M. Eichenfield *et al.*, Nat. Photon. **1**, 416 (2007).
[12] V. R. Almeida *et al.*, Nature (London) **431**, 1081 (2004).
[13] R. Espinola *et al.*, Opt. Express **12**, 3713 (2004).
[14] J. K. Ranka *et al.*, Opt. Lett. **25**, 25 (2000).
[15] W. Chen and D. L. Mills, Phys. Rev. Lett. **58**, 160 (1987); D. N. Christodoulides and R. I. Joseph, Phys. Rev. Lett. **62**, 1746 (1989); A. Aceves and S. Wabnitz, Phys. Lett. A **141**, 37 (1989); B. J. Eggleton, Phys. Rev. Lett. **76**, 1627 (1996); C. M. de Sterke and J. E. Sipe, Prog. Opt. **33**, 203 (1994).
[16] Y. Liu *et al.*, Phys. Rev. Lett. **99**, 153901 (2007).
[17] K. Kawano and T. Kitoh, *Introduction to Optical Waveguide Analysis* (Wiley, New York, 2001).
[18] N. Moiseyev and S. Freidland Phys. Rev. A **22**, 618 (1980).
[19] E. Narevivius and N. Moiseyev, Phys. Rev. Lett. **81**, 2221 (1998); **84**, 1681 (2000).
[20] M. V. Berry, Czech. J. Phys. **54**, 1039 (2004).
[21] B. Crosignani *et al.*, J. Opt. Soc. Am. **72**, 1136 (1982); A. Ciattoni *et al.*, *ibid.* **22**, 1384 (2005).
[22] O. Cohen *et al.*, Phys. Rev. Lett. **91**, 113901 (2003).
[23] X. Liu *et al.*, Phys. Rev. Lett. **82**, 4631 (1999).
[24] A. Szameit *et al.*, Phys. Rev. A **77**, 043804 (2008).
[25] Y. Silberberg, Opt. Lett. **15**, 1282 (1990).